ACS APPLIED MATERIALS & INTERFACES

Research Article

www.acsami.org

Molecular Mechanistic Origin of Nanoscale Contact, Friction, and Scratch in Complex Particulate Systems

Soroosh Jalilvand[†] and Rouzbeh Shahsavari*[,†,‡,§]

[†]Department of Civil and Environmental Engineering, [‡]Department of Material Science and NanoEngineering, and [§]Smalley Institute for Nanoscale Science and Technology, Rice University, Houston, Texas 77005, United States

Supporting Information

ABSTRACT: Nanoscale contact mechanisms, such as friction, scratch, and wear, have a profound impact on physics of technologically important particulate systems. Determining the key underlying interparticle interactions that govern the properties of the particulate systems has been long an engineering challenge. Here, we focus on particulate calcium−silicate−hydrate (C−S−H) as a model system and use atomistic simulations to decode the interplay between crystallographic directions, structural defects, and atomic species on normal and frictional forces. By exhibiting high material inhomogeneity and low structural symmetry, C−S−H provides an excellent system to explore various contact-induced nanoscale deformation mechanisms in complex particulate systems. Our findings provide a deep fundamental understanding of the role of inherent material features, such as van der Waals versus Coulombic interactions and the role of atomic species, in controlling the nanoscale normal contact, friction, and scratch mechanisms, thereby providing de novo insight and strategies for intelligent modulation of the physics of the particulate systems. This work is the first report on atomic-scale investigation of the contact-induced nanoscale mechanisms in structurally complex C−S−H materials and can potentially open new opportunities for knowledge-based engineering of several other particulate systems such as ceramics, sands, and powders and self-assembly of colloidal systems in general.

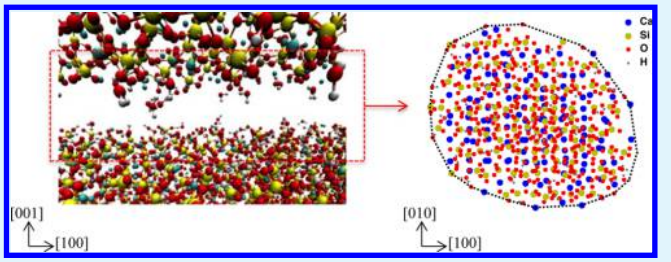

KEYWORDS: *nanoscale contact, friction, scratch, particulate systems, calcium silicates*

INTRODUCTION

Understanding interparticle interactions and nanoscale contact, such as nanoscale friction, scratch and wear, are among the key scientific and technological challenges associated with the physics of particulate systems. A fundamental understanding of this subject requires decoding the intricate chemomechanical coupling of well-defined interfaces with single-asperity contacts.[1−3] In this context, two views are proposed for treating the single-asperity contact at the atomic scale.[4,5] The first view assumes the tip as one single entity as in single-asperity laws of contact in the continuum theories. The second view belongs to an atomistic understanding of contact that treats every atom in the interface as a discrete unit whose collective behavior is interpreted in relation to multiasperity contact theories. This latter view was instrumental to explain the breakdown of continuum theories for single-asperity nanoscale contacts, for example, the contact of an amorphous carbon tip on diamond.[5,6]

Nanofriction is another important interparticle interaction that may arise from the sliding of two (or more) particles. While probing such interactions is experimentally quite difficult at the level of a few nanometers, molecular dynamic (MD) simulations of single-asperity contacts provide an alternative to understanding the detailed nanoscale mechanisms and interactions involved in nanoscale friction.[4,7,8] As an example, MD simulations at 0 K on sliding of rough deformable surfaces at different sliding speeds and surface roughness showed that friction increases with roughness and, due to surface flattening, it reduces to nearly zero after repetitive sliding.[8] A similar study illustrated that, while temperature has minimal effect when dealing with noncommensurate lattice alignments with limited adhesion, friction in adhesive, commensurate contacts tends to decrease with increasing temperature.[9]

As a particular class of nanofriction problems, scratch and wear phenomena at contacts of nanometer size have received considerable attention in the community.[10−12] An analytical relation between atomistic contact area and pileup-driven coefficient of friction was recently developed and verified with large-scale MD simulation.[13] Scratch simulation tests performed on samples of crystalline specimens (SiC and Cu) showed an increase in the value of scratch hardness with depth of cut, owing to dislocation pileup ahead of sliding.[11,12] Quite recently, it was shown that the scratch test could be used as a tool to determine the fracture toughness of a material via the theory of linear elastic fracture mechanics (LEFM).[14,15] The fracture toughness extracted from scratch experiments on a wide range of materials from polymers to metals and ceramics was shown to be in close agreement with conventional test

Received: September 17, 2014
Accepted: December 31, 2014

DOI: 10.1021/am506411h
ACS Appl. Mater. Interfaces XXXX, XXX, XXX−XXX

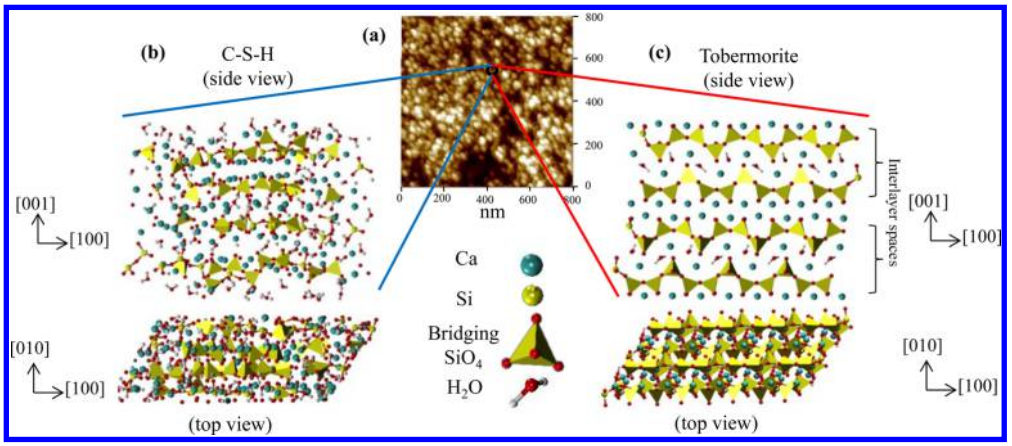

Figure 1. (a) An atomic force microscopy image of the surface of a particulate hydrated cement paste.[20] The nanogranular structure of the hydrated cement paste consists of particles with structures close to the amorphous-like C−S−H (b) and the crystalline tobermorite (c).

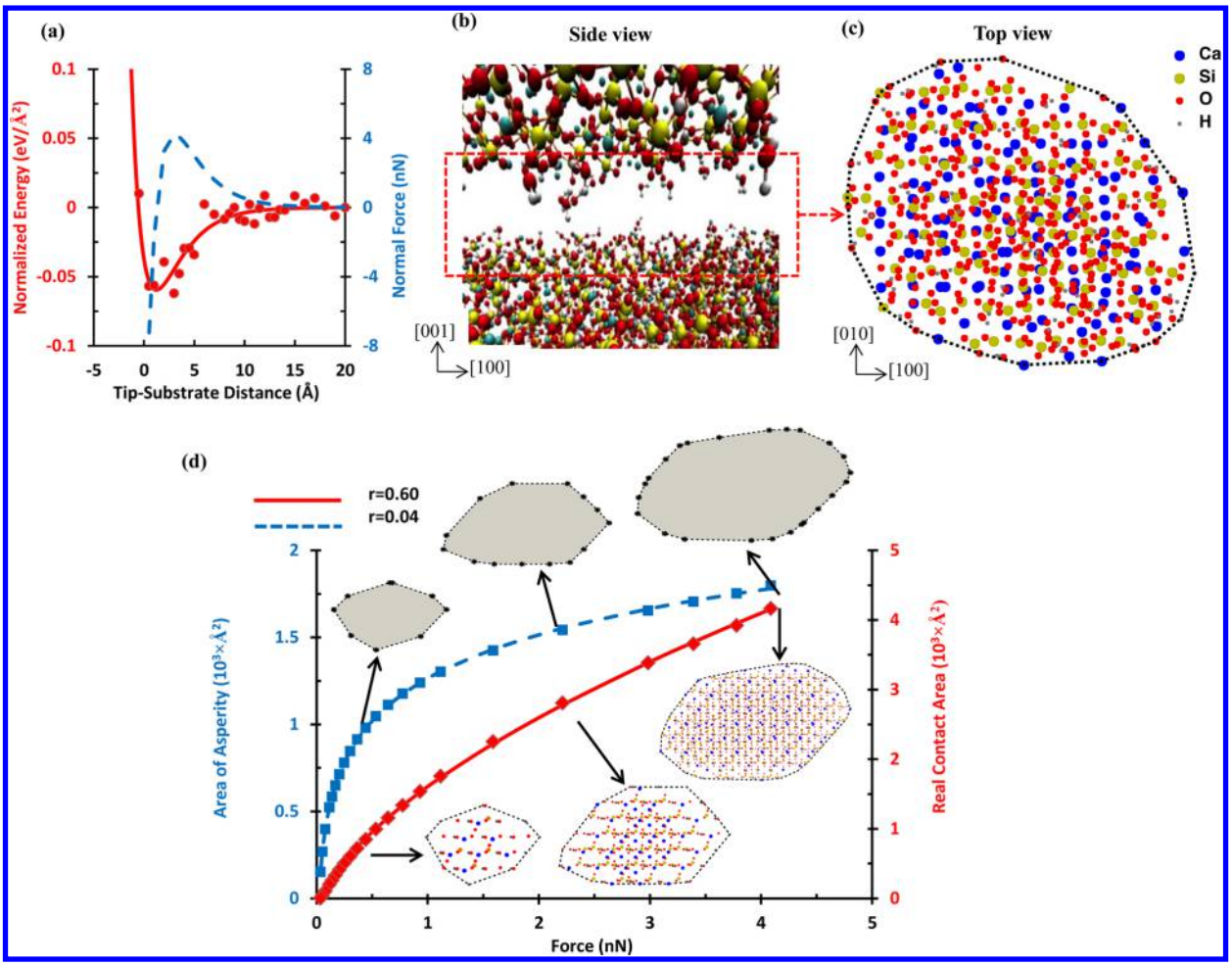

Figure 2. (a) Variation of the binding energy and the normal force between the tobermorite tip and substrate. Normal force between the tip and substrate (black line) is obtained as the derivative of the Morse function fitted to binding energy values. Positive values of the normal force correspond to attraction. The binding energy values are normalized with respect to the tip's area of contact ([001] surface). (b) A close-up side view of the contact region between the tip and the substrate, (c) the top view of the area of asperity in (b). The area of asperity is defined as the area of the smallest convex polygon that encloses the interacting substrate atoms. (d) Relation between the normal force and the two realizations of atomistic contact areas at the interface of tobermorite tip and substrate: the *real contact area* (red line), and the *area of asperity* (blue line).

results.[14,16,17] However, given the material inhomogeneity and atomic-scale nature of interactions, there is no unified understanding of the detailed mechanism involved in nanoscale contact. The problem is essentially unexplored for structurally complex systems where different atomic species make up the interfacial interactions. For instance, what is the role of each atom type on interparticle interactions and thus integrity of the particulate systems? Are there ways to tune the intrinsic material features at the level of individual particles through the knowledge of surface contact?

DOI: 10.1021/am506411h
ACS Appl. Mater. Interfaces XXXX, XXX, XXX−XXX

The objective of the present work is to study nanoscale surface contact in structurally complex materials, which are of both technological and scientific significance. We use molecular dynamic simulations to study a model system of calcium−silicate−hydrate (C−S−H) phase, which is the primary binding component and the main source of mechanical properties in the cement paste. This complex and variable stoichiometry compound is an amorphous mixture of CaO_2 (C), SiO_2 (S), and H_2O (H), which surrounds various crystalline phases in the hydrated cement.[18] Despite its appearance as the colloidal phase in the cement paste, C−S−H is considered as an assemblage of discrete nanoscale particles, which interact through normal and frictional forces (Figure 1).[19,20] As such, the overall properties of the C−S−H phase naturally depend on interparticle interactions, which are largely unexplored. Specially, the occurrence of random surface defects, such as SiO_2 vacancies on the surface of C−S−H particles or the existence of bridging Si tetrahedra (Figure 1b), break any symmetric pattern associated with interfacial sliding in crystalline interfaces observed earlier and complicates the nature of interactions. Therefore, C−S−H is an excellent system for our study to expand the current state of the knowledge on surface contacts to complex, low-symmetry systems.

The present article is structured as follows: First, we detail the influence of crystallographic directions and the realization of atomistic contact on attractive and repulsive interparticle forces in C−S−H and tobermorite, where the latter is a natural crystalline analog of C−S−H (Figure 1c). Next, we present the results of scratch simulation on tobermorite to predict the fracture toughness properties. Finally, we decouple the distinct contribution of the van der Waals (vdW) versus Coulombic interactions as well as the effect of various atomic species in nanoscale contact, followed by a short discussion and conclusion.

RESULTS AND DISCUSSION

Interparticle Interactions. *Effect of Particle Orientation.* The normalized binding energies of the biparticle system in C−S−H and tobermorite along different crystallographic directions are shown in Supporting Information, Figure S1. To provide quantitative comparison of the binding energies, we fitted a Morse potential to the data and used two descriptors: the "well depth" and "well width", where the latter corresponds to the inverse of the curvature term in Morse potential. It turns out that the effect of orientation on the binding energy (and for that matter, interparticle equilibrium distance and applied forces) is more pronounced for tobermorite than it is for C−S−H. The reasons go back to the more homogeneous behavior of C−S−H and are consistent with the structure of the two compounds; that is, compared to the crystalline, layered structure of tobermorite, the disordered structure of C−S−H makes its behavior rather insensitive to orientations. Accordingly, it is expected the binding energy descriptors such as well depth and well width show a more homogenized behavior in the case of C−S−H (Supporting Information, Figure S1d,e). In the case of tobermorite, it appears that the neighboring [010] planes have the maximum well depth and well width and thus maximum interactions among all interfaces. This is likely due to the most packed structure of tobermorite (i.e., direction of strong silicate chains), which is only slightly inclined to the [010] direction.

Realization of Atomistic Contact Area. Figure 2a illustrates the results of static energy minimization of tobermorite tip−substrate system at various separation distances. The binding energy is normalized with respect to the tip's area of contact along [001] directions. The normal force (dashed line in Figure 2a) is obtained as the derivative of the Morse function fitted to the binding energy values. As seen in Figure 2a, the attractive force dominates the tip−substrate interaction even at small distances. As the tip−substrate distance increases, the attractive force first reaches its peak value at ∼3 Å and then tends to decrease until it finally goes to zero at the cutoff distance for electrostatic interactions (i.e., 15 Å).

To relate atomistic findings to the laws of continuum contact a measure of contact area is required. Two definitions of nanoscale contact areas could be realized: the *area of asperity* (A_{asp}) and the *real contact area* (A_{real}).[4,5] The area of asperity is the area of the convex polygon that encloses all the interacting substrate atoms, while the real contact area is the number of substrate atoms (N_{at}) that fall within the range of chemical (short-range) interaction with the tip atoms, multiplied by a constant (A_{at}) representing the effective area of each substrate atom.

$$A_{real} = N_{at} \times A_{at} \tag{1}$$

In view of the larger cutoff distance of electrostatic interactions compared to vdW interactions, the choice of N_{at} in eq 1 is made by considering which substrate atoms fall within the cutoff range (15 Å) of Coulombic interaction with the tip atoms. Furthermore, the effective area of the substrate atoms (A_{at}) is assumed to be the same for all the atom types and is calculated based on the weighted average of the covalent radii of all the substrate atoms.

$$A_{at} = \sum_{Ca,Si,O,H} \frac{N_i}{\sum N_i} \pi R_i^{\,2} \tag{2}$$

In above, i denotes the various types of atoms (Ca, Si, O, and H) that exist in the substrate, R_i denotes the covalent radius of each atom type,[21] N_i is the number of substrate atoms that belong to a particular atom type category, and $\sum N_i$ is the total number of substrate atoms. On the basis of eq 2, the value of the effective atomic area (A_{at}) is estimated as 3.06 Å^2 in our calculations. By projecting all the interacting atoms into a common surface, A_{asp} is obtained as the area of the smallest convex polygon that encloses these atoms. Figure 2b,c shows a close-up side view and top view of A_{asp} of the tip and substrate; the top view demonstrates the schematics of the convex polygon that forms the A_{asp}.

To relate the normal force and the contact area, we adopt the power-law form of continuum single-asperity theories of contact[22−24]

$$A_{asp} = aL^r + b \quad (r < 1) \tag{3}$$

where L is the normal force and a, b, and r are the fitting parameters. Moreover, we choose to use only the intermediate part of the normal force plot where a monotonic variation can be observed (tip−substrate distance greater than 3 Å). According to the continuum single-asperity theories for nonadhesive and adhesive contacts,[22−24] the area of asperity (i.e., A_{asp}) varies sublinearly with respect to the normal load. Similar behavior is also observed in our simulations of adhesive contact where we obtain $r = 0.04$ (blue line in Figure 2d). Now if we express the contact area in eq 3 in terms of A_{real} (i.e., the

DOI: 10.1021/am506411h
ACS Appl. Mater. Interfaces XXXX, XXX, XXX−XXX

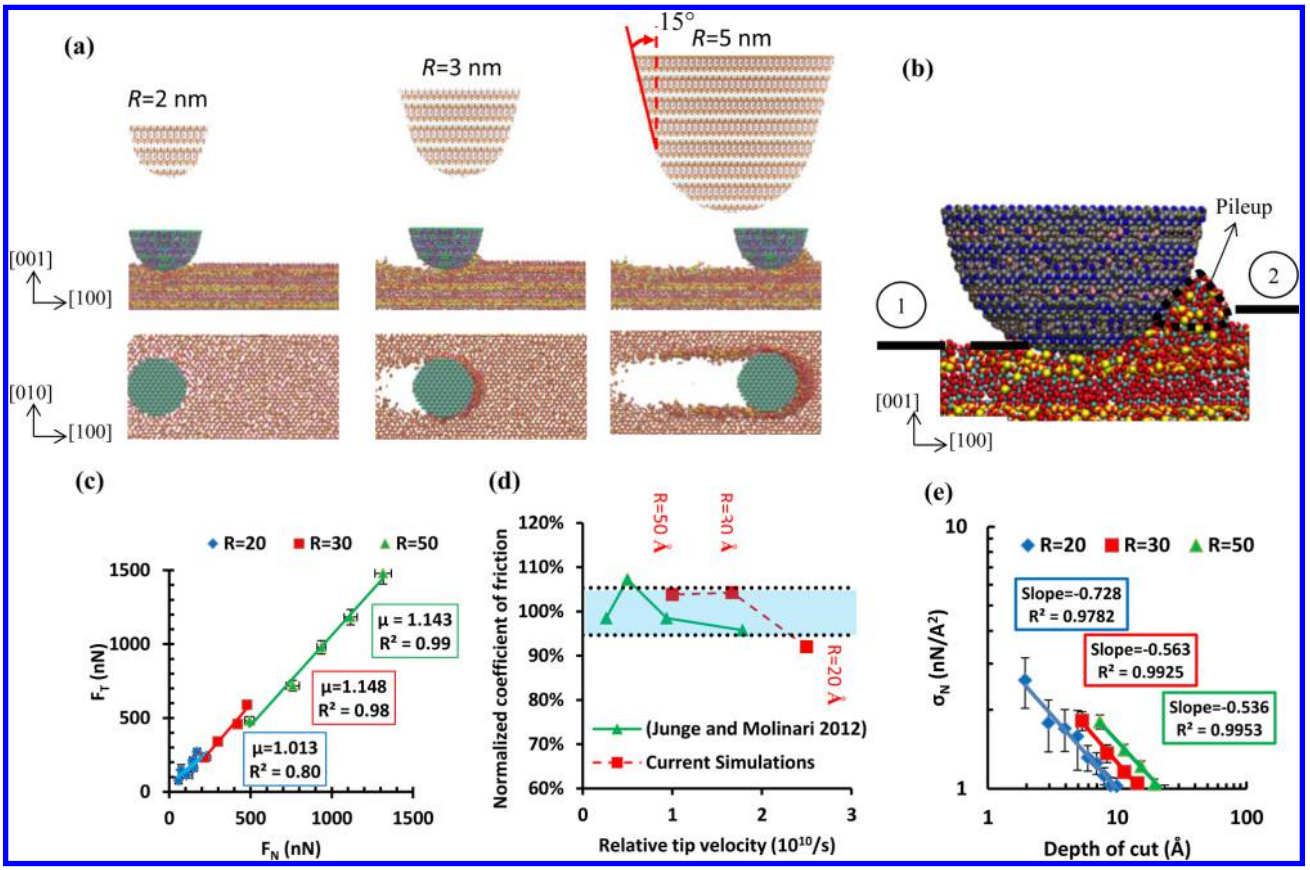

Figure 3. (a) Scratch simulation of tobermorite with spherical tips. Schematics of the formation of pileup ahead of the tip is clear as it slides on the substrate from left to right. Tips have conical shapes (with half angle 15°) that end in a spherical extremity. (b) Close-up view of the pileup region ahead of the tip. Depth of cut is measured as the difference between the elevations (1) and (2). We define elevation (1) as the height of lowermost atom of the tip and elevation (2) as the elevation that is higher than 99% of substrate atoms (prior to scratching). (c) Friction coefficients and linear relations between the friction and normal forces at the interface of tip and substrate. (d) Effect of tip velocity relative to the tip size on the coefficient of friction calculated from scratch simulation on tobermorite. For comparison, similar simulations previously reported on aluminum are also presented.[10] (e) The nominal stress varies linearly with the depth of cut. Slopes obtained at ca. −0.5 hint at the domination of LEFM as the failure mechanism.

number of interacting atoms), we observe a far less sublinear relation with r = 0.60 (red line in Figure 2d). Such a shift toward less sublinear behavior was also observed in the study of nonadhesive nanoscale contacts.[5] Furthermore, by considering A_{real} we can differentiate the role of each atom type on the normal forces, which will be discussed in the last section.

Nanoscratch. Simulation of scratch test is performed by sliding tips with spherical extremity of radius 2−5 nm on a tobermorite substrate (Figure 3a and Supporting Information, movie 1). Tips are assumed rigid and are cut from a bulk sample of tobermorite. The evolution of pileup in front of the tip is depicted in Figure 3a,b. Figure 3c shows a linear relationship between the friction and normal force and the friction coefficients obtained from scratch test simulations with various spherical tip sizes. Each point in Figure 3c is obtained by averaging the horizontal and vertical components of the interfacial forces over the steady-state period of sliding. Error bars indicate the fluctuations inherent to the sliding simulation. Similar linear trends were reported in the scratch simulations performed on SiC and aluminum.[10,13]

As the tip size increases, the data in Figure 3c become less scattered around the linear trend, and the predicted value for the friction coefficient shows convergence. Two simultaneous conditions contribute to this behavior. First, the larger depths probed with larger tip sizes provided a better statistical representation of friction and normal forces, which in turn, corresponded to less scatter in the data. Second, the use of identical sliding velocity (50 m/s) used for all the simulations caused different tip sizes to experience relatively different loading rates. To clarify the influence of the latter, Figure 3d demonstrates the effect of relative velocity of the tip on the coefficient of friction calculated from scratch simulations on tobermorite. For comparison, the effect of velocity on friction coefficient of aluminum via scratch simulations is also presented.[10] In each case, the coefficient of friction is normalized with respect to the average coefficient of friction calculated from all scratch simulations on the material. While rate dependency is not significant for tips with radius of 3 and 5 nm, the higher relative loading rate for the 2 nm tip radius causes slight reduction in the value of friction coefficient. An analogous behavior was also reported in the scratch simulations performed on aluminum using a spherical indenter of radius 2.3 nm and varying velocities.[10] Overall, the scatter in both sets of data is bounded to 5.3% standard deviation.

Prediction of Fracture Toughness from Scratch Simulations. One interesting outcome of nanoscratch test is to predict the fracture toughness of materials. To this end, we use the analytical relation that was recently proposed based on linear elastic fracture mechanics (LEFM) theory and has since been successfully applied to a set of microscale scratch

DOI: 10.1021/am506411h
ACS Appl. Mater. Interfaces XXXX, XXX, XXX−XXX

experiments on materials with a wide spectrum of fracture toughness from butter and parrafin wax to ceramics, metals, and cement paste.[14,15,17] In essence, this relations narrows to

$$F_{eq} = 4K_c d\sqrt{\frac{R\beta}{3}} \text{ where}$$
$$\beta\left(\alpha = \frac{d}{R}\right) = \sqrt{1+2\alpha} + \frac{1}{\sqrt{2\alpha}}\text{arcsinh}(\sqrt{2\alpha}) \quad (4)$$

where F_{eq} is a combination of friction force (F_T) and normal force (F_N) exerted on the tip; K_c is the fracture toughness, R is radius of the tip, d is depth of cut, and β is a dimensionless parameter. For a spherical tip, it can be shown that $F_{eq} = (F_T{}^2 + (665/1188)F_N{}^2)^{1/2}$.[14]

We follow the same convention in Akono et al.[14] to measure the depth of cut; that is, the depth of cut is measured with respect to the substrate level prior to scratching. We take this as the elevation higher than 99% of substrate atoms before scratching (elevation (2) in Figure 3b). Note that while we use the convention of Akono et al.[14] for calculation of depth of cut, we realize that in our atomistic analysis there is a significant contribution from pileup atoms (see Figure 3b) to resist the tip movement, which is not negligible. This issue will be addressed later by quantifying the contribution of pileup to the tip−substrate interaction.

In using eq 4 care should be taken in regard to size effects.[25] As stated earlier, the developments of Akono et al.[14] are based on LEFM. Therefore, it is important to verify the compliance of our data to the governing relations of LEFM before any meaningful data extraction for fracture toughness could be made. It is well-known of LEFM solutions that the nominal stress at failure varies inversely with the square root of structure size.[26] In the context of scratch tests, the former corresponds to the average bearing capacity (σ_N) at the tip front, and the latter is represented by the depth of cut (d).[25] More precisely, σ_N refers to the ratio of friction force (F_T) to the tip−substrate contact area projected on a vertical plane, for which we use the approximate relation provided in ref 17.

$$A_v = \frac{2}{3R}(2Rd)^{1.5} \quad (5)$$

When plotted in logarithmic scale, the linear relationship between σ_N and the inverse of $d^{1/2}$ is characterized by line with the slope from −1 to 2. To verify the existence of such relationship, the results of scratch simulations using the tips with radius of 2−5 nm are plotted in Figure 3e. Line fitting reveals slopes of −0.728, −0.563, and −0.536 for tips of radius 2, 3, and 5 nm, respectively. The resulting slopes are in good agreement with the characteristic value of −0.5 expected for LEFM solutions (the slight divergence of the values for the smallest tip size are likely due to higher loading rates discussed earlier).

The above argument regarding the compliance of scratch test data to the governing laws of LEFM could also be viewed in a more generalized framework of energetic size effect law (SEL). The energetic SEL bridges between two strength theories: (1) plastic theory, in which the nominal strength of the material is assumed to be independent of the structural size, and (2) fracture theory (LEFM), which considers a linear degradation in the nominal strength of material with respect to a characteristic length of structure.[15] The relation representing SEL was initially proposed in the study of fracture in concrete and rock[26] and has recently been adopted for the analysis of macroscopic scratch test data.[15,25]

$$\sigma_N = \frac{B\sigma_Y}{\sqrt{1+\frac{D}{D_0}}} \quad (6)$$

In the above equation, σ_N is the nominal strength of the material (measure of material stress state at failure), B is a dimensionless constant, σ_Y is the yield strength of material, D is a measure of structure size, and D_0 is the characteristic structure length. In the context of scratch test, σ_N is considered as the ratio of friction force (F_T) to the to the tip−substrate contact area (A_v).[25] Alternatively, σ_N could be defined in terms of the combination of friction and normal forces (F_{eq}) at the tip−substrate interface.[15] The former convention based on F_T is used in our analysis. Moreover, the structure size (D) is represented by the depth of cut (d) in view of the scratch test configurations.[15,25]

By applying the SEL in eq 6 to the material response in scratch test the governing strength theory could be located between the two limits: plastic-asymptote ($\sigma_N = B\sigma_Y$) that is independent of structure size, and LEFM-asymptote ($\sigma_N = B\sigma_Y(D_0)^{1/2}(D)^{-1/2}$) that varies inversely with the characteristic structure length. For the scratch test data to be informative of the fracture toughness property of the material, the data need to locate closer to the LEFM-asymptote in the SEL framework.[15,25] For this purpose, a linear regression is used in the form $Y = AX + C$, with $X = d$ and $Y = \sigma_N{}^{-2} = (F_T/A_v)^{-2}$, to obtain the SEL parameters $B\sigma_Y = 1/(C)^{1/2}$ and $D_0 = C/A$ for each tip size as shown in Table 1.[15]

Table 1. Size Effect Law Parameters for Each Tip Size Obtained from Performing Linear Regression to Scratch Simulations

tip radius R (nm)	A	C	D_0 (Å)	$B\sigma_Y$ (nN/Å^2)
2	0.0842	0.0110	0.131	9.535
3	0.0547	0.0146	0.267	8.276
5	0.0384	0.0268	0.698	6.108

Figure 4a shows the results of fitting the SEL relation in eq 6 to the data obtained from our nanoscratch simulations. The nanoscratch results are presented in terms of dimensionless parameters $\sigma_N/B\sigma_Y$ and D/D_0, and are presented together with the microscopic experimental scratch test data reported for the cement paste.[14,27] The experimental scratch test results were obtained using parallelepiped blades of widths 2.5−10 mm.[14,27] As can be observed in Figure 4a, the results of our nanoscratch simulations are more inclined toward the LEFM-asymptote. This elucidates the applicability of the LEFM-based formulation in nanoscratch simulations for predictive analysis of fracture toughness of materials.

For the remainder of this work, we focus on the analysis of the tip with radius 5 nm. This is the only case in which one complete depth of substrate unit cell (24.38 Å) is probed and thus is most representative. To obtain a first approximation to the fracture toughness in the tobermorite sample, the data from scratch simulation are fitted to eq 4 (Figure 4b). Accounting for the offset in the data fitting, that is, x_0 in the inset of Figure 4b representing the intersection of the fitted line with the x axis, we can obtain the value of fracture toughness for each depth of cut (Figure 4b). The results show a fracture toughness, K_c, close to 2.9 MPa·m$^{1/2}$ for tobermorite, which compares well

DOI: 10.1021/am506411h
ACS Appl. Mater. Interfaces XXXX, XXX, XXX−XXX

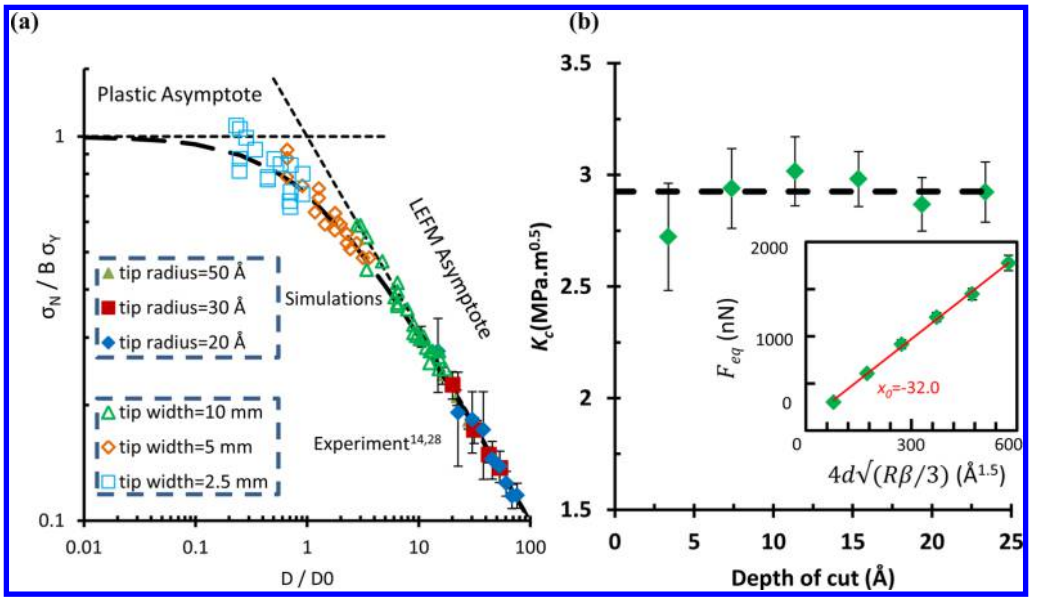

Figure 4. (a) The results of nanoscratch simulations closely follow the energetic size effect law along the LEFM-asymptote. A similar trend was previously observed for the microscopic scratch experiments on cement paste.[14,27] The results provide the justification for the use of nanoscratch simulation for the prediction of fracture toughness. (b) Fracture toughness predicted through fitting to the scratch simulation results (via eq 4). (inset) The intersection with the x-axis of the fitted line to eq 4 (x_0), which is used to predict individual fracture toughness values for each depth of cut.

with 0.66 MPa·m$^{1/2}$ and 0.67 MPa·m$^{1/2}$ obtained from scratch test and three-point bending experiments, respectively, on cement paste.[14,28] Note, however, that the fracture toughness reported in those works corresponds to microscopic (or perhaps macroscopic) realization of cement paste that represents a homogeneous material containing several hydration components such as C−S−H, portlandite, and even porosities and defects. In our study, however, cement paste is represented by uniform crystalline phase of tobermorite devoid of any impurity or porosity; hence, it is not surprising to obtain larger values of fracture toughness for this defect-free C−S−H crystal. However, still close level of agreement in the order of magnitude between simulations and experiments is quite encouraging.

Effect of Pileup. As stated earlier, eq 4 assumes that the only source of resistance against the movement of the tip comes from the material ahead of the tip and below the substrate level (elevation (2) in Figure 3b). In other words, the material resulted from chipping is no longer connected to the bulk of substrate and thus exerts no force on the sliding tip. In the atomistic view of scratch, however, substrate atoms are dislocated rather than chipped, and as they move to the pileup region, they still form a connected network that can resist against the tip movement. Figure 5a,b shows that the contribution of pileup to the total friction and normal force amounts to 40% and 30%, respectively. The data for normal force is more scattered for various tip sizes compared to friction force. This could be attributed to the fact that Coulombic interactions contribute more strongly to normal forces. This will be discussed in the next section.

van der Waals Versus Coulombic Interactions Controlling Physics of Particulate C−S−H. Differentiating the effect of vdW versus Coulombic interactions at the interface of the tip and substrate suggests the domination of vdW interaction in developing resistance to the horizontal movement of the tip (Figure 5c). Coulombic interactions, although insufficient in providing lateral resistance, contribute strongly to development of adhesion in normal direction between tip and substrate (Figure 5d). The underlying mechanism can be physically explained in the following way. In the non-equilibrium condition of sliding of the tip on the substrate, two simultaneous interactions are present: first, vdW interactions that are repulsive in nature and are activated by overclosure of several atomic species at the close neighborhood of the tip and substrate, and second, Coulombic interactions that are predominantly attractive and apply over a large region of substrate extending away from the tip. While the repulsive part of vdW interactions scales with r^{-12}, all of the Coulombic interactions scale with r^{-1}, suggesting the complete dominance of forces in the former (proportional to r^{-13}) compared to those of the latter (proportional to r^{-2}). Still, this absolute dominance is not exactly reflected in Figure 5d where the contribution from vdW interactions to the normal force is only at the ratio of 60 to 40 compared to Coulombic interactions (as clearly expressed in Figure 5f). The behavior is explained by the long-ranged nature of Coulombic interactions that results in the contribution of a larger number of substrate atoms compared to the short-ranged vdW forces (more precisely the repulsive part of vdW forces) that apply within a small neighborhood of the tip.

Despite the large contribution of Coulombic interactions to the normal tip−substrate forces, horizontal resistance on the tip is mainly composed of vdW interactions (see Figure 5e). The difference is explained by the relative position of the tip and substrate in the two cases and the adhesive nature of contact provided by Coulombic interactions. In the normal direction, all the substrate atoms are located on one side of the tip (bottom); therefore, the resultant Coulombic forces (that are adhesive) tend to add up, causing the tip to be attracted by the substrate (see Figure 5d). In the horizontal direction, however, the location of substrate atoms is not favored in any particular direction, and therefore the resultant Coulombic forces tend to cancel out. As the depth of cut increases, the distribution of substrate atoms becomes more biased in front of the tip

DOI: 10.1021/am506411h
ACS Appl. Mater. Interfaces XXXX, XXX, XXX−XXX

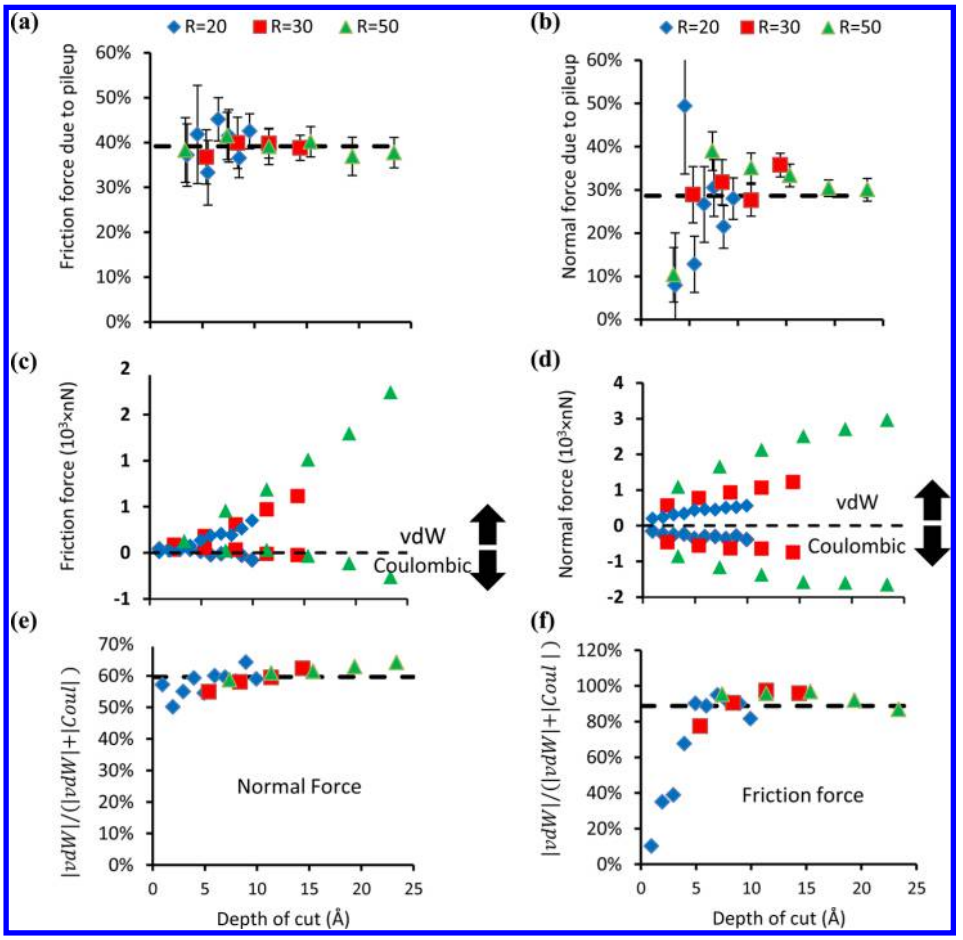

Figure 5. (a) Contribution of pileup to the tip−substrate friction force and (b) normal force. (c) Friction at the interface of tip and substrate is majorly dominated by repulsive van der Waals (vdW) interactions. (d) vdW and Coulombic interactions contribute to the development of repulsive and adhesive components of normal force, respectively. (e) The normal force at the interface of tip and substrate is favored by vdW interactions by a ratio of 60 to 40 compared to Coulombic forces. (f) The horizontal force at the tip−substrate interface is dominated strongly by interactions from vdW sources, giving them a 90 to 10 leverage compared to Coulombic interactions. (e, f) The symbol | | indicates absolute values.

(formation of pileup), and this explains the trend in Figure 5c where Coulombic interactions gradually tend to attract the tip toward the pileup.

Distinguishing the Effect of Various Atom Types. By distinguishing the effect of various atom types on the total vdW forces a pattern could be identified (see Table 2). Bridging

Table 2. Contribution of Various Atomic Species to the vdW and Coulombic Interactions Acting at the Interface of Tip and Substrate Both Made of Tobermorite

	average contribution				
ineraction force	Ca	Si	Ob−O[a]	Ow[b]	Hw[b]
normal (Coulombic)	25%	35%	70%	6%	4%
normal (vdW)	16%	12%	63%	9%	0%
friction (vdW)	23%	5%	63%	10%	0%

[a]Ob−O: oxygen atoms forming the silicate chain. [b]Hw and Ow: hydrogen and oxygen atoms in water molecules.

(Ob) and end oxygen (O) atoms are contributing the most, then Ca, Si, and Ow (oxygen of water molecules). Figure 6 shows this trend for both friction and normal forces. Contribution of different atoms to Coulombic forces follows almost the same pattern except that the roles of Si atoms are more prominent. Only normal forces are considered with

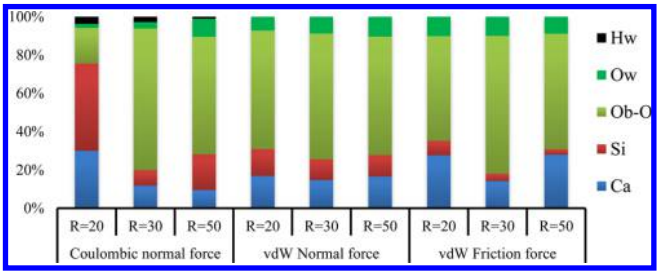

Figure 6. Contribution of various atom types to the tip−substrate interactions. Hw and Ow are hydrogen and oxygen atoms in water molecule. Ob−O and Si are the oxygen and silicon atoms forming the silicate chain, and Ca corresponds to inter- and intralayer calcium. Contribution of different atom types is quantified in terms of both vdW and Coulombic interactions.

reference to Coulombic interactions because this is the main direction for Coulombic contribution compared to vdW contributions as discussed in the previous section. According to Figure 6, in the case of Coulombic forces, the contribution of individual atom types is affected more strongly with variation in the tip size (and consequently indentation depth) compared to the case of vdW forces. This could be attributed to the positive/negative nature of Coulombic interactions that depend on atomic charges, and as a result small variations in the local

DOI: 10.1021/am506411h
ACS Appl. Mater. Interfaces XXXX, XXX, XXX−XXX

configuration or size of the region could change the resulting force on an atom from repulsive to attractive.

Overall, our results show that despite the fact that the number of Ca atoms is equal to the number of Si atoms (i.e., Ca/Si = 1), Ca atoms contribute more strongly to the interparticle forces and scratch and fracture resistance compared to Si atoms. Thus, while Si atoms (and in general silica chains) play the dominant role for integrity of the individual C−S−H particles,[18,20,29] Ca atoms are more crucial for interparticle interactions and thus for the integrity of the whole particulate C−S−H assembly. This finding is novel and a significant result of this paper related to intrinsic feature of the tobermorite family. It suggests that increasing the ratio of Ca/Si toward more realistic C−S−H (e.g., the average Ca/Si in real C−S−H is ∼1.6−1.7),[30] would considerably increase the fracture toughness of C−S−H, provided that the backbone structure of tobermorite or local atomic environment are not dramatically altered. Indeed, recent advanced analysis via combinatorial molecular optimization of defects in C−S−H have shown that Ca/Si = 1.5 provides the maximum fracture toughness in C−S−H among all possible stoichiometries from Ca/Si ≈ 1 to 2.1.[31] Beyond Ca/Si = 1.5, it was shown that the backbone silica layer becomes significantly distorted, leading to major network disconnectivity and thus reduction in strength and fracture toughness. By distinguishing the role of different atomic species, our analysis provides a deep physical insight into the root causes of this pattern.

DISCUSSION

Understanding the complex chemomechanical interactions that govern the behavior of particulate systems such as C−S−H requires the study of well-defined interfaces across multiple scales. This article addressed this issue through the study of C−S−H and its closest crystalline analog (i.e., tobermorite) at three distinct scales:

1. At the smallest scale, we looked at the interparticle interfaces through an atomistic lens. The contact area at the interface of two particles was defined in terms of the number of interacting atoms, and the relation between the normal force and this "atomistic" notion of contact area was established. Similar relationship was also derived between the normal force and the "macroscopic" notion of contact area (i.e., single asperities). It was demonstrated that atomistic realization of the contact correlated more linearly with respect to the normal interaction force.
2. In an intermediate scale, we considered the interparticle interaction not through the study of individual atoms but by looking at the collective behavior of the system of atoms within the particle. To this end, we used the binding energy and its descriptors: energy well depth and well width to study the behavior of a biparticle system. The effect of particle orientation on the overall energy of the system was considered, and configurations with highest and lowest energy levels were determined. It was demonstrated that the biparticle system of the amorphous C−S−H is less sensitive to the relative orientation of particles compared to tobermorite. Moreover, it was shown that two tobermorite particles form a more stable configuration when they approach along the [010] axes and are less stable when connected along the [001] axes (Supporting Information, Figure S1c).
3. In the largest scale considered here, we performed scratch simulation on a large supercell of tobermorite. The collective behavior of several hundred thousand atoms was integrated in the form of friction and normal forces, which were used for the calculation of friction coefficient. Furthermore, interpretation of the scratch simulation results in the context of energetic SEL provided a direct link between the atomistic interactions and macroscopic fracture toughness property. It was demonstrated that the results of nanoscratch simulation were applicable to LEFM-based formulas and could be used for prediction of fracture toughness. Table 3 presents the value of fracture toughness predicted for tobermorite from nanoscratch simulations and compares the result with the fracture toughness parameters previously reported for cement pastes.

Table 3. Comparison of the Fracture Toughness Values Obtained from Current Simulation on Tobermorite and Previously Reported Experiments on the Cement Paste

simulation[a]		experiment[a]	
before pileup correction	after pileup correction	scratch test[14,27]	3-point bending test[32]
2.9 ± 0.1	1.7 ± 0.06	0.66 ± 0.05	0.62−0.66

[a]All values are in MPa·m$^{0.5}$ units.

The predicted fracture toughness for tobermorite is a few times larger than its macroscopic representation. The difference is understandable as tobermorite corresponds to an idealized pure crystalline cement paste without impurities, porosities, cracks, etc. Moreover, the LEFM-based formulation used for the prediction of fracture toughness assumes no resistance from the pileup of material in front of the tip. This resistance is quantified to be up to 40% in our scratch simulations. Therefore, adjusting for this effect, the fracture toughness prediction is reduced by 40% to yield 1.7 MPa·m$^{0.5}$, which is in closer agreement with experimental measurements for the cement paste. Finally, we demonstrated that the vdW (vs Coulombic) interactions has a more dominant role in nanoscale contact (including normal and frictional forces), and thus governs the mechanics and integrity of the particulate C−S−H systems. In this context, Ca atoms were revealed to play a key role in interparticle interactions of the system, unlike the individual particles where both Si and Ca atoms are key players in structural integrity.

In view of the similarities that exist between tobermorite and C−S−H and also because of the simplicity that the former crystalline structure provides, most of the analyses in this study were conducted using tobermorite unit cells. While we believe that the general trends obtained in this work are very insightful about the nature of interactions in the C−S−H particulate system, a complete understanding of these phenomena will require consideration of C−S−H unitcells and reactive ReaxFF force fields, which will be the subject of future research.

CONCLUSIONS

We studied the problem of nanoscale contact, friction and scratch, across different crystallographic directions, using a particulate model of C−S−H. We found that adhesive/repulsive normal interaction between two C−S−H particles is less sensitive to the crystallographic orientations compared to those of the layered crystalline tobermorite. We showed that

DOI: 10.1021/am506411h
ACS Appl. Mater. Interfaces XXXX, XXX, XXX−XXX

the contact area scales with 0.6 power of the normal force; that is, $A_{asp} \approx L^{0.6}$ when considering the multiasperity realization of the contact area, whereas this scaling is far more sublinear in the single-asperity (continuum) contact area where $A_{asp} \approx L^{0.04}$. This underscores the inherent differences in "nanoscale" versus "continuum" theories of contact and the need for elaborate analysis when adopting continuum theories for nanoscale granular materials.[4,5]

Scratch simulations on the interface of two tobermorite particles identified the coefficient of friction ~1 and demonstrated a linear relationship between the friction force and normal force. We predicted the inherent fracture toughness of tobermorite to be ~1.7 MPa·$m^{1/2}$, which is readily comparable with experiments, 0.66−0.67 MPa·$m^{1/2}$, on cement paste.[14,27,32] Unlike the micro/macro-scratch tests in which the cementitious materials are typically chipped away ahead of the tip, there is a significant pileup in nanoscale scratch simulations that contribute up to 40% of the resistance force.

Finally, the ratios of vdW to Coulombic contributions to the friction and normal forces in C−S−H were found to be ~9 and 1.5, respectively, indicating pronounced contribution of the vdW forces. By distinguishing the inherent contribution of each atom type, we found that despite the fact that the number of Ca atoms is equal to Si atoms in tobermorite, Ca species contribute more to the nanoscale contact, wear, fracture toughness, and interparticle interactions. This finding, which is in contrast to the level of individual particles where silica chains are key to structural integrity, suggests that increasing the Ca/Si ratio will improve the fracture toughness and the interparticle interactions of C−S−H (provided that the backbone of individual particles are not dramatically changed). This finding may provide de novo concepts and strategies for an intelligent tuning of the mechanics of particulate systems; that is, the modulation must be done both at the level of individual nanoparticles (e.g., via tuning the Si topology[31]) and interparticle interactions (e.g., via increasing the Ca content). To our knowledge, this work is the first report of atomistic-scale analysis of contact and scratch simulations in structurally complex particulate systems and can open new opportunities to understand other nanoscale phenomena such as indentation-induced mechanisms in cement[40,41] and tuning its mechanical properties in hybrid particulate systems.[42−44] Broadly, it can impact the physics and self-assembly of other particulate systems such as ceramics, sands, powders, grains, and colloidal systems.

EXPERIMENTAL SECTION

To model the C−S−H, we used the so-called consistent molecular model of C−S−H that is based on a set of bottom-up atomistic simulations.[30] The resulting unit cell reproduces the NMR data of actual C−S−H, and has C/S of 1.65 and density of 2.65 g/cm^3, which are close to the values obtained by SANS measurement (C/S = 1.7, density = 2.6 g/cm^3). The model has a chemical composition of $(CaO)_{1.65}(SiO_2)(H_2O)_{1.75}$ with a triclinic crystal size of 13.06 × 29.02 × 23.08 Å^3 and angles α = 87.8°, β = 91.7°, and γ = 122.7°. The tobermorite unit cell that was employed here has a chemical composition of $Ca_6Si_6O_{18}\cdot 2H_2O$ and a monoclinic crystal structure with dimensions of 6.59 × 7.39 × 24.38 Å^3 and angles α = 90°, β = 90°, and γ = 123.88° (i.e., so-called 11 Å tobermorite).[33]

To properly describe interatomic interactions in both C−S−H and tobermorite, CSH-FF potential was used in all MD simulations.[34] This empirical force field is developed by optimization of partial charges and Leonard-Jones parameters against ab initio calculations on tobermorite and has been highly successful in reliably predicting structural (lattice parameters and bond distances) and mechanical properties (elastic constants) of C−S−H and tobermorite family.[34] Furthermore, CSH-FF has proven both adequate and computationally efficient in simulation of water confined in small pores inside C−S−H grains.[35] The detailed parameters and equations of CSH-FF potential are given in Supporting Information. One can also use other potentials for scratch tests,[45] but care must be taken in assessing the predictive capability of potentials with respect to mechanical properties.[34]

Both normal and friction forces were considered in the study of interparticle interactions. The normal force was evaluated as the derivative of the binding energy in the C−S−H (or tobermorite) biparticle system, and the friction force is obtained as the resistance between the tobermorite tip and substrate in a scratch test setup. The analysis of the normal force involved two parts: first, we used MD simulation to explore the effect of various interfaces on the binding energy of the C−S−H (or tobermorite) biparticle system. For this purpose, two identical particles were immersed in water with density 1 g/cm^3, and the energy of the system was incrementally calculated when the particles approached each other along one of [100] or [010] or [001] directions (see Supporting Information, Figure S1a). Here, C−S−H particles were represented by a nonperiodic 1 × 2 × 1 supercell, and tobermorite particles were represented with a nonperiodic 5 × 5 × 1 sueprcell. In the second part, we only focused on the weakest surface that is more likely for decohesion (and thus reserve as particle boundaries during crystal growth processes) and studied the relation between the atomistic contact area and the interparticle forces through static energy minimization, as implemented in the GULP package.[36] More precisely, a 3 × 3 × 1 tobermorite supercell was gradually brought into contact with a tobermorite substrate of size 9 × 9 × 1, and the energy of the system was calculated at each increment. Periodic and nonperiodic boundary conditions were imposed in the directions parallel ([100] and [010]) and normal ([001]) to the substrate plane, respectively. To avoid relative tip−substrate displacement, a few Si atoms were kept fixed in the upper and lower layer of the tip and the substrate.

The analysis of friction and wear phenomenon was performed using the MD simulation of scratch test between a spherical tip and substrate both being cut from a bulk tobermorite sample. The tip had a conical shape (with half angle 15°) that ended in a spherical asperity. Radius of curvature of the tip (R = 2−5 nm) characterizes the tip size, and consequently, the range in which the depth of cut can vary (d = 0.1−2.5 nm). Depth of cut is defined as the distance between bottom elevation of the tip and top elevation of the substrate: the latter corresponds to the elevation that is higher than 99% of substrate atoms (elevation (2) in Figure 3b), and the former refers to the elevation of the lowermost atom of the tip (elevation (1) in Figure 3b). In all the scenarios, the tip height is adjusted to eliminate the effect of boundary conditions. Substrate dimension in the direction of tip movement is chosen to allow for a minimum sliding distance of 5 × R (R being the radius of curvature of the tip); the same rule as in tip height applies to the other two dimensions of the substrate. As an example, for the tip of radius 5 nm and height 8 nm, a 62 × 32 × 3 supercell is used as the substrate; the total number of atoms in this case is on the order of 500 000. Periodic and nonperiodic boundary conditions are imposed in lateral and normal directions of the substrate surface, respectively. Tip atoms are made infinitely rigid and move at a constant velocity with respect to the substrate, thereby preserving the initial conformation of tip throughout the sliding. The bottom silica chain of the substrate is kept fixed throughout the simulation to avoid relative tip−substrate displacement. Throughout the simulation, the system temperature was maintained at ~1 K to exclude the influence of any thermally activated processes.

To perform friction and scratch tests, first we conducted the MD simulation of indentation. The tip kept penetrating into the substrate at a constant velocity until it reached a specified maximum depth of cut (half of the tip radius). As the tip passed through different substrate layers, snapshots of the position and velocity of atoms were stored. These data represented restarting points each corresponding to a specific depth of cut, which later went through MD relaxation to finally set the stage for sliding simulation at desired depth. The cutting depth

DOI: 10.1021/am506411h
ACS Appl. Mater. Interfaces XXXX, XXX, XXX−XXX

varied among various simulations based on the tip size. In all cases, sliding continued until the tip reached to the end of the substrate (e.g., for the 5 nm tip size mentioned earlier the simulation takes 600 ps). Finally, the friction and normal forces were obtained from scratch simulation by averaging the horizontal and vertical components of the interfacial forces between tip and substrate atoms during the steady-state period of sliding.

All MD simulations were performed by LAMMPS code at temperature 1 K.[37] Positions and velocities were sampled from a canonical ensemble (NVT) with Nose-Hoover thermostat.[38] A typical time step of 1 fs was employed in all the simulations except for the cases with very small interparticle distances where a time step of 0.005 fs was adopted. All the simulations continued until they reached steady state. All atomic visualizations are produced using the molecular graphics program VMD.[39]

■ ASSOCIATED CONTENT

Supporting Information

Illustration of normalized binding energies, details of the parameters and equations of the CSH-FF potential., and a movie of a scratch simulation test depicting pile up formation. This material is available free of charge via the Internet at http://pubs.acs.org.

■ AUTHOR INFORMATION

Corresponding Author

*E-mail: rouzbeh@rice.edu.

Author Contributions

R.S. designed the research; S.J and R.S performed the research; S.J. analyzed the data; and S.J. and R.S. wrote the paper.

Notes

The authors declare no competing financial interest.

■ ACKNOWLEDGMENTS

We acknowledge support from National Science Foundation (NSF) Grant Nos. CMMI-1235522 and 1346506. The use of supercomputer machines for this work was supported in part by National Insitutes of Health Award No. NCRR S10RR02950 and an IBM Shared University Research (SUR) Award in partnership with CISCO, Qlogic, and Adaptive Computing, and in part by the Data Analysis and Visualization Cyber infrastructure funded by NSF under Grant No. OCI-0959097.

■ REFERENCES

(1) Szlufarska, I.; Chandross, M.; Carpick, R. W. Recent Advances in Single-Asperity Nanotribology. *J. Phys. D: Appl. Phys.* **2008**, *41*, 123001.

(2) Luan, B.; Robbins, M. O. Contact of Single Asperities with Varying Adhesion: Comparing Continuum Mechanics to Atomistic Simulations. *Phys. Rev. E: Stat., Nonlinear, Soft Matter Phys.* **2006**, *74*, 026111.

(3) Yang, C.; Persson, B. N. J. Molecular Dynamics Study of Contact Mechanics: Contact Area and Interfacial Separation from Small to Full Contact. *Phys. Rev. Lett.* **2008**, *100*, 024303.

(4) Mo, Y.; Szlufarska, I. Roughness Picture of Friction in Dry Nanoscale Contacts. *Phys. Rev. B: Condens. Matter Mater. Phys.* **2010**, *81*, 035405.

(5) Mo, Y.; Turner, K. T.; Szlufarska, I. Friction laws at the nanoscale. *Nature* **2009**, 1116−1119.

(6) Binquan, L.; Mark, O. R. The Breakdown of Continuum Models for Mechanical Contacts. *Nature* **2005**, *435*, 929−932.

(7) Yang, C.; Persson, B. N. J. Contact Mechanics: Contact Area and Interfacial Separation from Small Contact to Full Contact. *J. Phys.: Condens. Matter* **2008**, *20*, 215214.

(8) Spijker, P.; Anciaux, G.; Molinari, J.-F. Dry Sliding Contact Between Rough Surfaces at the Atomistic Scale. *Tribol. Lett.* **2011**, *44*, 279−285.

(9) Spijker, P.; Anciaux, G.; Molinari, J. F. Relations Between Roughness, Temperature and Dry Sliding Friction at the Atomic Scale. *Tribol. Int.* **2013**, *59*, 222−229.

(10) Junge, T.; Molinari, J. F. Molecular Dynamics Nano-Scratching of Aluminium: A Novel Quantitative Energy-Based Analysis Method. *Procedia IUTAM* **2012**, *3*, 192−204.

(11) Mishra, M.; Szlufarska, I. Analytical Model for Plowing Friction at Nanoscale. *Tribol. Lett.* **2012**, *45*, 417−426.

(12) Mishra, M.; Szlufarska, I. Dislocation Controlled Wear in Single Crystal Silicon Carbide. *J. Mater. Sci.* **2013**, *48*, 1593−1603.

(13) Mishra, M.; Egberts, P.; Bennewitz, R.; Szlufarska, I. Friction Model for Single-Asperity Elastic-Plastic Contacts. *Phys. Rev. B: Condens. Matter Mater. Phys.* **2012**, *86*, 045452.

(14) Akono, A. T.; Ulm, F. J. Scratch Test Model for the Determination of Fracture Toughness. *Eng. Fract. Mech.* **2011**, *78*, 334−342.

(15) Akono, A.-T.; Ulm, F.-J.; Bažant, Z. P. Discussion: Strength-to-Fracture Scaling in Scratching. *Eng. Fract. Mech.* **2014**, *119*, 21−28.

(16) Thomas, J. J.; James, S.; Ortega, J. A.; Musso, S.; Auzerais, F.; Krakowiak, K. J.; Akono, A. T.; Ulm, F. J.; Pellenq, R. J. M. In *Fundamental Investigation of the Chemical and Mechanical Properties of High-Temperature-Cured Oilwell Cements*, Proceedings of the Offshore Technology Conference, Houston, TX, U.S.A, 30 April−3 May, Offshore Technology: Richardson, TX, 2012; pp 3277−3287.

(17) Akono, A.-T.; Ulm, F.-J. Fracture Scaling Relations for Scratch Tests of Axisymmetric Shape. *J. Mech. Phys. Solids* **2012**, *60*, 379−390.

(18) Taylor, H. F. W. Nanostructure of C-S-H: Current Status. *Adv. Cem. Based Mater.* **1993**, *1*, 38−46.

(19) Constantinides, G.; Ulm, F. J. The Nanogranular Nature of C-S-H. *J. Mech. Phys. Solids* **2007**, *55*, 64−90.

(20) Nonat, A. The Structure and Stoichiometry of C-S-H. *Cem. Concr. Res.* **2004**, *34*, 1521−1528.

(21) Cordero, B.; Gomez, V.; Platero-Prats, A. E.; Reves, M.; Echeverria, J.; Cremades, E.; Barragan, F.; Alvarez, S. Covalent Radii Revisited. *Dalton Trans.* **2008**, 2832−2838.

(22) Hertz, H. Ueber die Berührung Fester Elastischer Körper. *J. Reine Angew. Math.* **1882**, *1882*, 156−171.

(23) Schwarz, U. D. A Generalized Analytical Model for The Elastic Deformation of An Adhesive Contact Between a Sphere and a Flat Surface. *J. Colloid Interface Sci.* **2003**, *261*, 99−106.

(24) Maugis, D. Adhesion of spheres: The JKR-DMT Transition Using a Dugdale Model. *J. Colloid Interface Sci.* **1992**, *150*, 243−269.

(25) Lin, J.-S.; Zhou, Y. Can Scratch Tests Give Fracture Toughness? *Eng. Fract. Mech.* **2013**, *109*, 161−168.

(26) Bažant, Z. P. Size Effect in Blunt Fracture: Concrete, Rock, Metal. *J. Eng. Mech., ASCE* **1984**, *110*, 518−535.

(27) Akono, A. T.; Reis, P. M.; Ulm, F. J. Scratching as a Fracture Process: From Butter to Steel. *Phys. Rev. Lett.* **2011**, *106*, 204302.

(28) Cotterell, B.; Mai, Y. W. Crack Growth Resistance Curve and Size Effect in the Fracture of Cement Paste. *J. Mater. Sci.* **1987**, *22*, 2734−2738.

(29) Shahsavari, R.; Buehler, M. J.; Pellenq, R. J. M.; Ulm, F.-J. First-Principles Study of Elastic Constants and Interlayer Interactions of Complex Hydrated Oxides: Case Study of Tobermorite and Jennite. *J. Am. Ceram. Soc.* **2009**, *92*, 2323−2330.

(30) Pellenq, R. J. M.; Kushima, A.; Shahsavari, R.; Van Vliet, K. J.; Buehler, M. J.; Yip, S.; Ulm, F. J. A Realistic Molecular Model of Cement Hydrates. *Proc. Natl. Acad. Sci. U. S. A.* **2009**, *106*, 16102−16107.

(31) Abdolhosseini Qomi, M. J.; Krakowiak, K. J.; Bauchy, M.; Stewart, K. L.; Shahsavari, R.; Jagannathan, D.; Brommera, D. B.; Baronnet, A.; Buehler, M. J.; Yip, S.; Ulm, F. J.; Van Vliet, K. J.; Pellenq, R. J. M. Combinatorial Molecular Optimization of Cement Hydrate. *Nat. Commun.* **2014**, *5*, 4960.

(32) Hu, X.; Wittmann, F. Size Effect on Toughness Induced by Crack Close to Free Surface. *Eng. Fract. Mech.* **2000**, *65*, 209−221.

DOI: 10.1021/am506411h
ACS Appl. Mater. Interfaces XXXX, XXX, XXX−XXX

(33) SA, H. The Crystal Structure of The 11A Natural Tobermorite. *Z. Kristallogr.* **1981**, *154*, 189−198.
(34) Shahsavari, R.; Pellenq, R. J. M.; Ulm, F.-J. Empirical Force Fields for Complex Hydrated Calcio-Silicate Layered Materials. *Phys. Chem. Chem. Phys.* **2011**, *13*, 1002−1011.
(35) Youssef, M.; Pellenq, R. J. M.; Yildiz, B. Glassy Nature of Water in an Ultraconfining Disordered Material: The Case of Calcium-Silicate-Hydrate. *J. Am. Chem. Soc.* **2011**, *133*, 2499−2510.
(36) Gale, J. D.; Rohl, A. L. The General Utility Lattice Program (GULP). *Mol. Simul.* **2003**, *29*, 291−341.
(37) Plimpton, S. Fast Parallel Algorithms for Short-Range Molecular Dynamics. *J. Comput. Phys.* **1995**, *117*, 1−19.
(38) Shinoda, W.; Shiga, M.; Mikami, M. Rapid Estimation of Elastic Constants by Molecular Dynamics Simulation Under Constant Stress. *Phys. Rev. B: Condens. Matter Mater. Phys.* **2004**, *69*, 134103.
(39) Humphrey, W.; Dalke, A.; Schulten, K. VMD: Visual Molecular Dynamics. *J. Mol. Graphics* **1996**, *14*, 33−38.
(40) Shahsavari, R.; Ulm, F.-J. Indentation Analysis of Fractional Viscoelastic Solids. *J. Mech. Mater. Struct.* **2009**, *4*, 523−550.
(41) Shahsavari, R., Chen, L. Screw Dislocations in Complex, Low Symmetry Oxides: Structures, Energetics and Impacts on Crystal Growth. *ACS Appl. Mater. Interfaces* **2015**, In Revision.
(42) Sakhavand, N.; Muthuramalingam, P.; Shahsavari, R. Toughness Governs the Rupture of Interfacial H-bond Assemblies at a Critical Length Scale in Hybrid Materials. *Langmuir* **2013**, *29*, 8154−163.
(43) Rafiee, M. A.; Narayanan, T. N.; Hashim, D. P.; Sakhavand, N.; Shahsavari, R.; Vajtai, R.; Ajayan, P. M. Hexagonal Boron Nitride and Graphite Oxide Reinforced Multifunctional Porous Cement Composites. *Adv. Funct. Mater.* **2013**, *23*, 5624−5630.
(44) Shahsavari, R. Hierarchcial Modeling of Structure and Mechanics of Cement Hdrates, Ph.D. Thesis, MIT, Cambridge, MA, 2011.
(45) Heinz, H.; Lin, T. J.; Mishra, R. K.; Emami, F. S. Thermodynamically Consistent Force Fields for the Assembly of Inorganic, Organic, and Biological Nanostructures: The INTERFACE Force Field. *Langmuir* **2013**, *29*, 1754−1765.

DOI: 10.1021/am506411h
ACS Appl. Mater. Interfaces XXXX, XXX, XXX−XXX